NJC

ROYAL SOCIETY OF CHEMISTRY

PAPER

View Article Online
View Journal | View Issue

Cite this: *New J. Chem.*, 2021, **45**, 9967

The effect of supports on hydrogenation and water-tolerance of copper-based catalysts†

Zheng Chen, * Xueying Zhao, Shuwei Wei, Dengfeng Wang and Xuelan Zhang*

Received 29th October 2020,
Accepted 30th April 2021

DOI: 10.1039/d0nj05302c

rsc.li/njc

The effect of supports (SiO_2, ZnO, ZrO_2 and Al_2O_3) on the hydrogenation and water-tolerance of copper catalysts were studied at reaction condition containing water. The copper catalysts with different supports showed different hydrogenation and water-tolerance performances. The result of XRD, BET, Raman, TPR, XPS, N_2O titration and TEM confirmed the interactions between copper and supports, and the formation of Cu–M_xO_y (M = Zn, Zr, and Al) interfaces had great effects on the catalytic activity and water-tolerance performance. In particular, too strong interactions suppressed the reduction of copper oxides, resulting in a low catalytic activity. Nevertheless, the formation of Cu–M_xO_y could provide more active sites, which provided more chances for the reactants to touch the active sites. By this method, the loss of active sites due to competitive adsorption between water and ethyl acetate could be made up, so that the water-tolerance of copper catalysts was improved.

1. Introduction

With the development of clean utilization of coal and biomass, the catalytic hydrogenation reaction of some specific compounds originating from coal or biomass have attracted considerable attention among researchers.[1–3] In these catalytic hydrogenation reactions, copper-based catalysts have been widely used due to their good selective hydrogenation of C=O bonds and relatively low activity for C–C bond hydrogenolysis.[4,5] Nonetheless, the particle size of the copper species, the dispersion of metal copper and the interaction effects between copper and the supports were the key factors affecting the catalytic performance of Cu-based catalysts. These factors depended greatly on the selection of supports with different surface properties. Although the same preparation method was used, copper-based catalysts possessed different physicochemical properties due to the use of different supports. At present, the effects of supports on the catalytic performance have been extensively researched by changing metal dispersion, surface area, oxygen storage capacity, basicity, and interactions between active species and support of the catalysts.[6–14] However, to the best of our knowledge, the effect of supports on the water-tolerance of copper-based catalysts has not been systematically researched so far.

In the process of clean utilization of coal and biomass, the production of ethanol was extensively researched due to its widespread use in chemical, energy, pharmaceutical and food industries. Recently, the hydrogenation of ethyl acetate to ethanol has attracted considerable attention.[15,16] This method had the advantages of high selectivity towards ethanol, low production cost and convenient operation, and could also solve the overcapacity problem of ethyl acetate. However, water impurities might exist in ethyl acetate during the hydrogenation reaction due to the non-ideal selectivity or raw materials derived from industrial scrap. Therefore, it is worth investigating that how the supports affect the hydrogenation and water-tolerance of copper catalysts. Simultaneously, our previous study has demonstrated that the doping of Zn into the Cu/SiO_2 catalyst could effectively improve the hydrogenation water-tolerance of Cu/SiO_2.[17] Moreover, a published study had also confirmed that water easily promoted the growth of copper particles, which led to the deactivation of the catalyst.[18] The strong interactions between copper and the support can hinder the particle growth in the reaction. Therefore, a strong interaction is beneficial for the enhancement of the water-tolerance of copper-based catalysts. ZrO_2 and Al_2O_3 have been widely used as support materials of copper catalysts.[19] The metal-support interaction can be enhanced due to the existence of surface coordinatively unsaturated Al^{3+} and $Zr^{4+}O^{2-}$.[20] ZrO_2- and Al_2O_3-supported copper catalysts have been used in CO and CO_2 hydrogenation, which showed high activity and hydrothermal stability.[21,22] Therefore, SiO_2, ZnO, ZrO_2 and Al_2O_3 were used as supports to study the effects of supports on the water-tolerance of copper-based catalysts.

In this study, the hydrogenation of ethyl acetate to ethanol was selected to study the influence of supports (SiO_2, ZnO, ZrO_2 and Al_2O_3) on the hydrogenation water-tolerance performance

College of Chemistry, Chemical Engineering and Materials Science, Zaozhuang University, Zaozhuang 277160, Shandong, China. E-mail: chenzhengtt@163.com, mhszxl@sxicc.ac.cn

† Electronic supplementary information (ESI) available: Physicochemical property characterization of Cu/SiO_2 is given in Figures S1–S5. See DOI: 10.1039/d0nj05302c

of copper-based catalysts. The obtained hydrogenation results were associated with characterizations to reveal the essence of the affection of the supports on the hydrogenation water-tolerance performance. We aimed at understanding the advantages of different supports for copper catalysts at reaction condition containing water, which is beneficial for researchers to develop highly efficient water-tolerant catalysts.

2. Experimental

2.1. Material

Copper(II) nitrate hydrate, aluminum nitrate nonahydrate, zinc nitrate hexahydrate, zirconium oxychloride octahydrate, tetraethyl orthosilicate, ethyl alcohol absolute and ammonium bicarbonate were bought from Sinopharm Chemical Reagent Co., Ltd. All reagents used in this study were of analytically pure grade and used without further purification.

2.2. Catalyst preparation

Copper catalysts were prepared by precipitation using ammonium bicarbonate as the precipitant. The obtained catalysts were marked as Cu/SiO_2, Cu/ZrO_2, Cu/ZnO and Cu/Al_2O_3 on the basis of different supports. The nominal copper loading of the catalysts was 25%.

For copper catalysts, 6.05 g of $Cu(NO_3)_2{\cdot}3H_2O$ was dissolved in the mixture of 50 ml deionized water and 50 ml ethanol. Then, $C_8H_{20}O_4Si$ (53.72 g), $Al(OH)_3{\cdot}9H_2O$ (32.38 g), $Zn(NO_3){\cdot}6H_2O$ (16.08 g) and $ZrOCl_2{\cdot}8H_2O$ (11.51 g) were added in 6 portions to the mixed solution under agitation, respectively, until they completely dissolved. Subsequently, 6 portions of a 200 ml NH_4HCO_3 aqueous solution with different concentrations were added into the above-mentioned mixed solutions under agitation. Finally, the mixed solutions were stirred for 3 h at 90 °C, and then aged for 12 h.

Thereafter, the mixtures were filtered and dried at 80 °C for 12 h. The obtained precursors were calcined at 400 °C in a muffle furnace for 4 h, and then pelletized, shed and sieved to 40–60 meshes.

The detailed information of the characterization methods and hydrogenation reaction conditions of all catalysts can be found in the ESI.†

3. Result and discussion

3.1. Characterization of the catalysts

Fig. 1 shows the XRD profiles of the Cu/SiO_2, Cu/Al_2O_3, Cu/ZnO and Cu/ZrO_2 catalysts to analyse their crystal structure and phases. For the Cu/SiO_2 and Cu/Al_2O_3 catalysts, there were no obvious peaks corresponding to the copper species observed, indicating that the copper species was highly dispersed. Just weak and broad characteristic peaks of SiO_2 (2θ = 22°, PDF#29-0085)[4,23] and Al_2O_3 (2θ = 34.8° and 64.9°, PDF#52-0803) were found, respectively. For the Cu/ZrO_2 and Cu/ZnO catalysts, the characteristic peaks of CuO, located at 35.2° and 38.5° (PDF#44-0706), could be clearly observed.[4,24] Other characteristic peaks

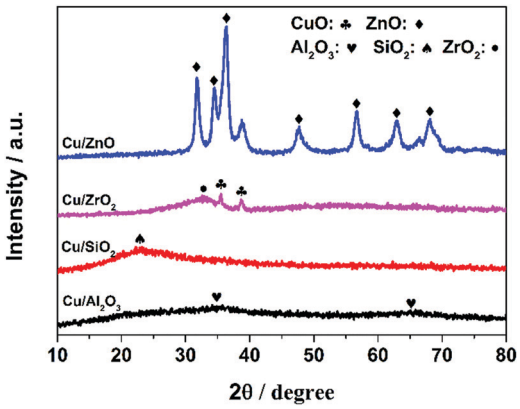

Fig. 1 XRD profiles of the Cu/SiO_2, Cu/Al_2O_3, Cu/ZnO and Cu/ZrO_2 catalysts.

were assigned to ZrO_2 (PDF#49-1746) and ZnO (PDF#36-1451), respectively.

The Brunauer–Emmett–Teller (BET) specific surface area and BJH adsorption pore size distribution of all catalysts were measured *via* N_2 adsorption–desorption measurements, and the relative results are shown in Fig. 2 and Table 1. Fig. 2a shows the adsorption–desorption isotherms, and it was clear that physisorption isotherms with hysteresis loops were different from each other. According to the IUPAC Classification, the Cu/SiO_2 catalyst was of type III, and the hysteresis loops belonged to the H3 type with aggregates of plate-like particles giving rise to slit-shaped pores; Cu/ZrO_2 and Cu/Al_2O_3 catalysts were of type II, and the hysteresis loops belonged to the H4 type with narrow slit-like pores; and Cu/ZnO catalyst was of type V, and the hysteresis loops belonged to the H2 type with ''ink bottle'' pores.[25,26] These results indicated that the copper catalysts with different supports possessed different pore features. From Fig. 2b, the most probable distributions of pore sizes were 18.1 and 6.5 nm for the Cu/ZnO and Cu/Al_2O_3 catalysts, suggesting the existence of mesopores. The distribution of pore sizes was concentrated on 10–200 nm or larger, indicating that mesopores and macropores existed in the Cu/SiO_2 catalyst. The BJH pore size distribution of the Cu/ZrO_2 catalyst was focused on 1.8 and 115 nm, suggesting that micropores and large-pores were present. Although the peak intensity of the pore size distribution for the Cu/ZnO catalyst was stronger than that of others, its pore sizes were bigger than the particle size (Fig. 5). This result indicated that the accumulation of particles was the formation reason of the pores.

The Raman spectra of the as-prepared catalysts were recorded to study the effects of the support on the molecular structure of CuO. As presented in Fig. 3a, the block CuO showed three peaks in the range of 50–1000 cm^{-1}, which were assigned to the A_g mode (282.8 cm^{-1}) and B_g mode (332.5 and 616.7 cm^{-1}) of CuO.[29] It was clear that the three peaks of CuO moved to lower wavenumbers when the supports were used, indicating that an interaction existed between the supports and CuO.[30] However, the Raman shift was also influenced by the particle sizes. A published study confirmed that particle growth

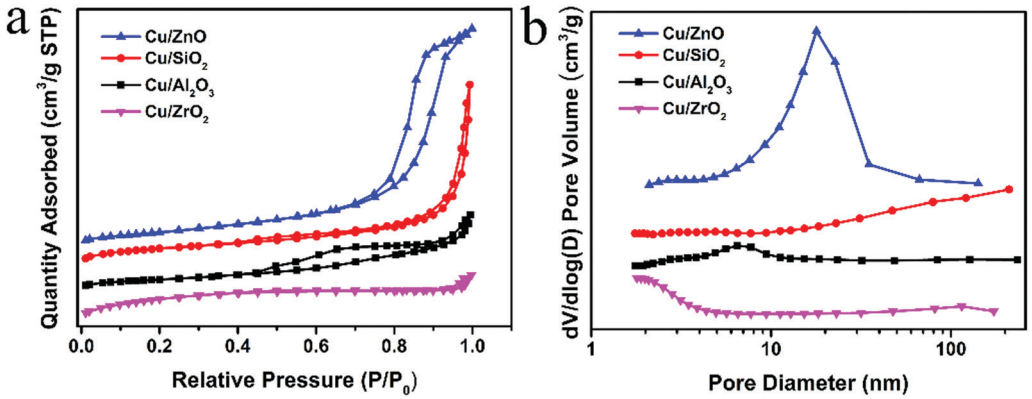

Fig. 2 (a), N_2 adsorption–desorption isotherms and (b), BJH adsorption pore size distribution for all catalysts.

Table 1 The textural properties of copper catalysts from BET and N_2O titration

Catalysts	S_{BET} (m^2 g_{cat}^{-1})	V_P (cm^3 g_{cat}^{-1})	S_{Cu} (m_{Cu}^2 g_{cat}^{-1})	D_{Cu} (%)	d_{Cu}^a (nm)
Cu/SiO_2	40.7	0.07	33.0	19.5	5.1
Cu/ZnO	41.0	0.16	24.5	14.5	6.9
Cu/Al_2O_3	26.0	0.04	14.3	8.4	11.9
Cu/ZrO_2	55.9	0.03	7.7	4.5	22.0

S_{Cu} = 1353 Y/X, D_{Cu} = 2 Y/X, d_{Cu}^a = 0.5 X/Y. X = the area of the TPR1 peak and Y = the area of the TPR2 peak, which determined by N_2O titration.[27,28]

would lead to Raman peaks move towards higher wavenumbers.[31] In our study, the particle size of the as-prepared catalysts had a big difference, which could be confirmed by TEM (Fig. 5). Therefore, the Raman shift could not totally show the size of interactions for the catalysts with different particle size. The following characterization explains it further.

Fig. 3b shows the profiles of H_2-TPR, indicating that the reduction temperatures of different catalysts had a great distinction. For Cu/SiO_2 and Cu/ZnO catalysts, a main reduction peak along with a shoulder could be observed, which were located at 240, 258 °C and 219, 248 °C, respectively. These reduction peaks could be assigned to the reduction of Cu^{2+} to Cu^+, and then to Cu^0. For the Cu/ZrO_2 catalyst, except for the peak assigned to the reduction of Cu^{2+} (233 °C), the peak at 303 °C corresponded to the reduction of the center of bulk copper oxide, and an additional peak (476 °C) could also be found, which was assigned to the reduction of Cu^{2+} with strong interactions between Cu and Zr.[32] Moreover, a broad reduction peak was also observed at 423 °C for the Cu/Al_2O_3 catalyst, which was attributed to the reduction of the bulk copper oxide phase. From the result of TPR, it was referred that the particle size of copper species in the Cu/Al_2O_3 and Cu/ZrO_2 catalysts was larger than that of the Cu/SiO_2 and Cu/ZnO catalysts, which was confirmed by TEM (Fig. 5 and Fig. S1, ESI†).

The specific surface area (S_{Cu}), average volume-surface diameter (d_{Cu}) and dispersion (D_{Cu}) of metal copper were measured by N_2O titration. The typical N_2O titration profiles are shown in Fig. 4, and the results calculated by a relative formula[27,28] were summarized in Table 1. From Fig. 4, it was clearly observed that there were two peaks for TPR2 of the Cu/Al_2O_3 and Cu/ZrO_2 catalysts, which distinguished that of the Cu/SiO_2 and Cu/ZnO catalysts. More specifically, Cu^{2+} could be reduced absolutely for the Cu/SiO_2 and Cu/ZnO catalysts by TPR1, and just one peak (180 °C), which was assigned to the reduction of Cu^+, could be found from TPR2. For the Cu/Al_2O_3 and Cu/ZrO_2 catalysts, except for the peak assigned to the reduction of Cu^+ at 200 °C, another peak could be found from TPR2, which

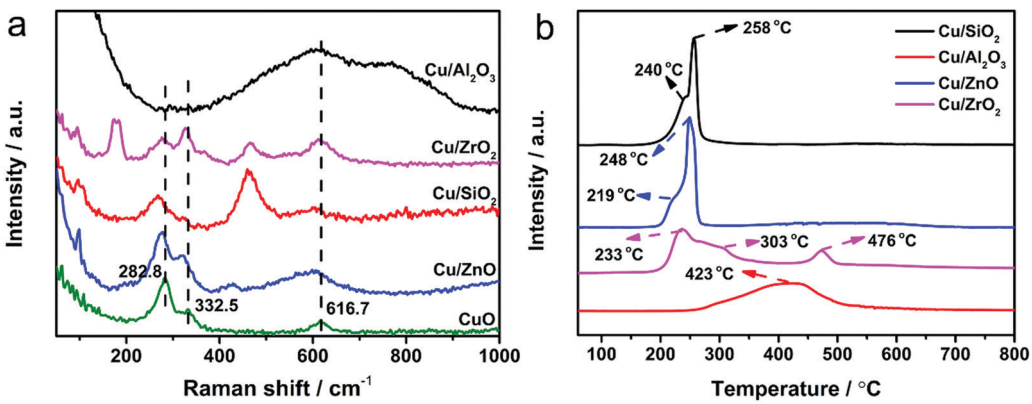

Fig. 3 (a) Raman spectra and (b) TPR pattern of bulk CuO and the prepared copper catalysts.

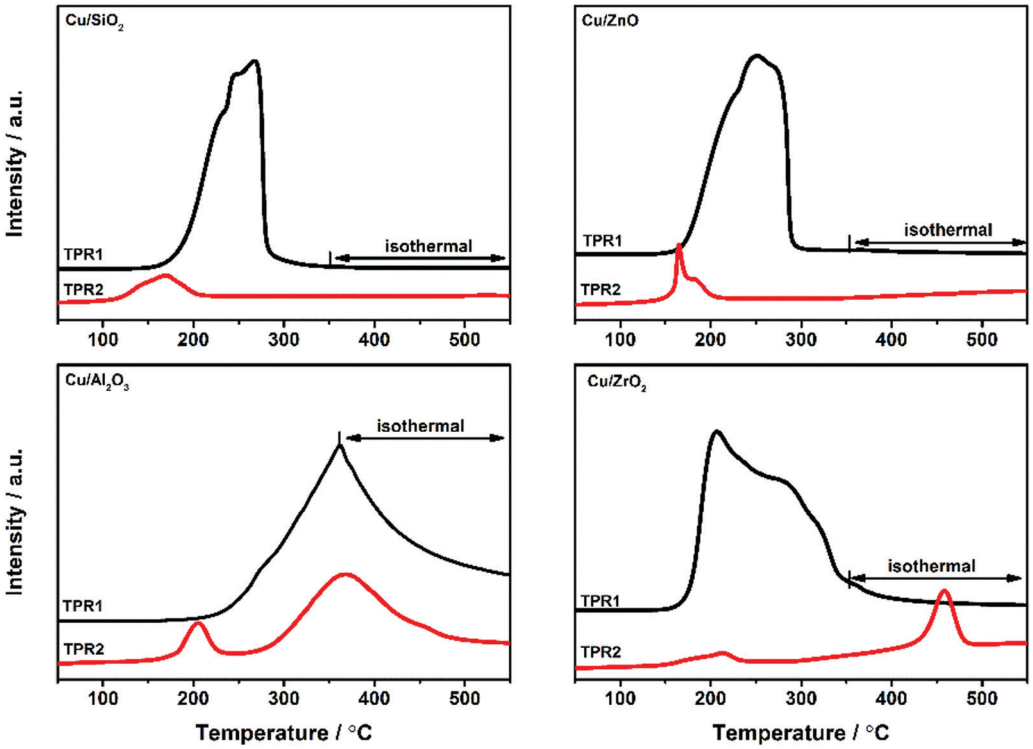

Fig. 4 TPR profiles of copper catalysts before and after N_2O oxidation at 50 °C.

corresponded to the reduction of Cu^{2+}. For the Cu/Al_2O_3 catalyst, the big particle size was responsible for the peak at 360 °C in TPR2 because its reaction temperature was basically in line with the reduction temperature of TPR1. Therefore, the peak at 360 °C in TPR2 was assigned to the reduction of the center of bulk copper oxide for the Cu/Al_2O_3 catalyst. However, the reduction temperature of another peak was 460 °C in TPR2 for the Cu/ZrO_2 catalyst, which was much higher than the reduction temperature in TPR1. Therefore, it was referred that the strong interaction between Cu and Zr was responsible for this reduction peak. That is, the strong interaction suppressed the reduction of partial Cu^{2+} under the conditions of the N_2O titration (350 °C, 40 min), and these Cu^{2+} ions could be reduced at 460 °C in TPR2. Therefore, just the first peaks belonged to the reduction of Cu^{+} for the Cu/Al_2O_3 and Cu/ZrO_2 catalysts. Based on the above-mentioned analysis, the S_{Cu}, d_{Cu} and D_{Cu} of reducible copper under the conditions of N_2O titration were calculated, and the result is shown in Table 1. From Table 1, it was found that S_{Cu} followed the order of Cu/SiO_2 (33.0 m^2 g_{cat}^{-1}) > Cu/ZnO (24.5 m^2 g_{cat}^{-1}) > Cu/Al_2O_3 (14.3 m^2 g_{cat}^{-1}) > Cu/ZrO_2 (7.7 m^2 g_{cat}^{-1}). Clearly, the strong interaction and the large particle size hindered the reduction of partial Cu^{2+}, so that Cu/Al_2O_3 and Cu/ZrO_2 had a little S_{Cu} as compared to that of Cu/SiO_2 and Cu/ZnO after the reduction.

Table 2 Binding energies of Cu $2p_{3/2}$ on the studied samples

Sample	Cu/SiO_2	Cu/Al_2O_3	Cu/ZnO	Cu/ZrO_2
Cu_1^{2+} (eV)	933.5	933.6	933.0	933.4
Cu_2^{2+} (eV)	935.8	935.2	934.0	934.5
$Cu_1^{2+}/(Cu_1^{2+}+Cu_2^{2+})^a$ (%)	35.8	18.6	38.8	15.6

[a] Percent of relative amount of the metal species evaluated by XPS.

The XPS of the Cu/SiO_2, Cu/Al_2O_3, Cu/ZnO and Cu/ZrO_2 catalysts were also performed, and the relative results are shown in Table 2 and Fig. S2 (ESI†). From Fig. S2 (ESI†), two peaks could be observed from about 935.2 and 955.5 eV, along with the satellite peaks of 2p → 3d at about 943.4 and 963.7 eV for all catalysts, indicating the existence of Cu^{2+}[3,33,34] Moreover, it was clear that the binding energies of Cu $2p_{3/2}$ could be deconvoluted into two symmetric peaks (Fig. S2, ESI†), indicating the existence of two Cu^{2+} species with different valence states. From Table 2, it was found that two types of Cu^{2+} centered around 935.0 (Cu_1^{2+}) and 933.5 eV (Cu_2^{2+}). The binding energies at around 933.5 eV were assigned to Cu^{2+} in the CuO species. The binding energies at around 935.0 eV, which indicated charge transfer from Cu^{2+} toward the supports, were assigned to Cu^{2+} with strong interaction with the supports.[35,36] Moreover, $Cu_1^{2+}/(Cu_1^{2+} + Cu_2^{2+})$ was calculated to show the relative content of two types of Cu^{2+}. In particular, the values of $Cu_1^{2+}/(Cu_1^{2+} + Cu_2^{2+})$ were 35.8, 18.6, 38.8 and 15.6% for Cu/SiO_2, Cu/Al_2O_3, Cu/ZnO and Cu/ZrO_2 catalysts, respectively, which indicated the relative content of the CuO species on the catalyst surface. That is, the order of the relative content of Cu^{2+} with a strong interaction with the support was Cu/ZrO_2, Cu/Al_2O_3, Cu/SiO_2 and Cu/ZnO. Therefore, Cu/ZrO_2 and Cu/Al_2O_3 were more difficult to be reduced than the Cu/ZnO and Cu/SiO_2 catalysts, which was also in agreement with the results

of TPR (Fig. 3b). From the above, it was inferred that the different supports had a different effect on the interactions between Cu and supports.

The TEM images of the spent catalysts before and after the ethyl acetate hydrogenation under reaction condition containing 5 wt% water are shown in Fig. 5 and Fig. S1 (ESI†). From Fig. 5a, it was found that copper species were distributed evenly before the reaction, and the particle sizes were mainly concentrated in 3–5 nm. Furthermore, although the particle sizes increased after the reaction (7–9 nm), the copper species were still highly dispersed on the silica supports for Cu/SiO_2, as shown in Fig. 5b. For the Cu/ZnO catalyst, the copper species were dispersed on the ZnO particles with sizes of 11–22 nm (Fig. 5c). The particle sizes also increased after the reaction for Cu/ZnO (18–36 nm), as shown in Fig. 5d. In addition, the sheet structure of the Cu/SiO_2 catalyst was in accordance with the result of BET that slit-shaped pores were found due to the aggregates of plate-like particles. For the Cu/ZnO catalyst, obvious channel structures could be observed from Fig. S3 (ESI†). However, the particle sizes of the Cu/ZrO_2 and Cu/Al_2O_3 catalysts were larger than that of the Cu/SiO_2 and Cu/ZnO catalysts, which can be found in Fig. S1 (ESI†). This result was in agreement with the result of TPR, and it was bad for the catalytic performance.

3.2. Catalytic results

The hydrogenation performance of the copper catalysts was evaluated to study the effects of supports on the gas-phase hydrogenation of ethyl acetate with 5 wt% water (Fig. 6a), and the calibration graphs of the products are shown in Fig. S3 (ESI†). It was found that the conversion of ethyl acetate increased with the increase in the reaction temperature.

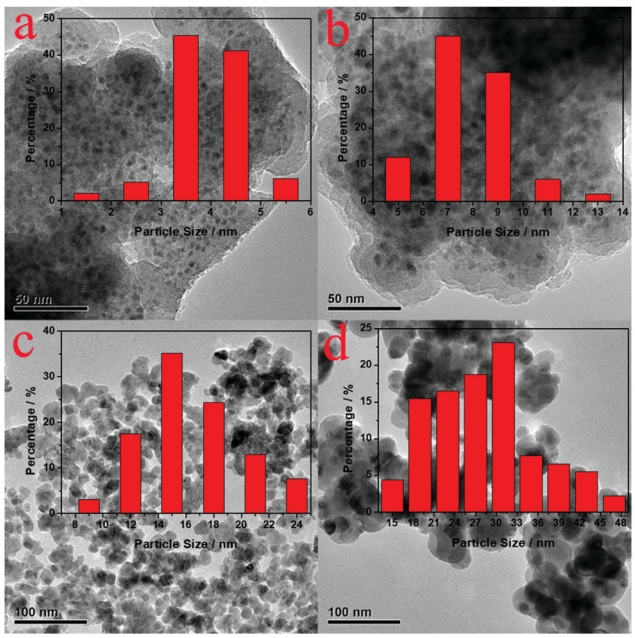

Fig. 5 The TEM images of Cu/SiO_2 (a and b) and Cu/ZnO (c and d) catalysts before (a and c) and after (b and d) the reaction.

For the Cu/Al_2O_3 and Cu/ZnO catalysts, the conversion of 95% was obtained, when reaction temperature was 280 °C, suggesting a good hydrogenation performance. Nonetheless, the selectivity of ethanol for the Cu/ZnO catalyst was higher than that of the Cu/Al_2O_3 catalyst, and the main by-product was ethane. Moreover, the conversion of ethyl acetate for the Cu/ZnO catalyst was also higher than that of the Cu/Al_2O_3 catalyst at each temperature. In particular, above 90% conversion was obtained for the Cu/ZnO catalyst at 240 °C, while the conversion of the Cu/Al_2O_3 catalyst was just 38%. Moreover, the turnover frequency (TOF) was calculated to further show the effects of the supports on the catalytic hydrogenation in the presence of water (Fig. 6b). It was clear that the TOF increased with the of the reaction temperature. Although the TOF of the Cu/Al_2O_3 catalyst increased from 1.72 to 28.03 h^{-1} (above 90% conversion), a high reaction temperature was necessary. For the Cu/ZnO catalyst, the value of TOF was 14.38 h^{-1} at 220 °C, and further increased to 16.18 h^{-1} with above 90% conversion at 240 °C. These results showed that the Cu/ZnO catalyst had better catalytic performance and water-tolerance. Therefore, the Cu/ZnO catalyst was chosen to evaluate its stability at 240 °C at reaction condition containing 5 wt% water, and the relative result is shown in Fig. S4 (ESI†). From Fig. S4 (ESI†), there was no apparent inactivation observed within 200 h for the conversion and ethanol selectivity of Cu/ZnO, suggesting that it had a good stability.

In order to confirm that the reason of low catalytic performance was due to the existence of water rather than the catalyst essential nature, the hydrogenation performances of all catalysts were evaluated at reaction condition no-containing water, as shown in Fig. 7 and Fig. S5 (ESI†). Except for the reaction temperature, other reaction conditions were the same. In particular, the reaction temperature of the Cu/ZnO catalyst was 240 °C, and the reaction temperature for other catalysts was 280 °C. From Fig. 7, it was found that 90% conversion was obtained for the Cu/ZnO catalyst at a reaction temperature of 240 °C. Although 87% conversion can be observed for Cu/SiO_2, and it required a reaction temperature of 280 °C. For the Cu/Al_2O_3 and Cu/ZrO_2 catalysts, their conversion increased with the reaction time. In particular, the conversions of the Cu/Al_2O_3 and Cu/ZrO_2 catalysts increased from 70 to 87% and from 25 to 79% within 50 h, respectively.

The above results from Fig. 6 and Fig. 7 indicated that 90% conversion can be obtained for the Cu/ZnO catalyst under two reaction conditions (240 °C), suggesting that the water had only a little effect on the activity of the Cu/ZnO catalyst. However, an obvious effect on the activity of the Cu/SiO_2 catalyst is that the conversion markedly decreased, as observed in Fig. 6 and Fig. 7.

3.3. Discussion

From Fig. 7, all catalysts showed a good hydrogenation performance. However, the Cu/Al_2O_3 and Cu/ZrO_2 catalysts had an induction period within 50 h. This may be because of the existence of strong interactions between Cu and Al_2O_3 or ZrO_2, and the big particle size, which had been confirmed by XPS, N_2O titration, TPR and TEM, led partial copper oxide

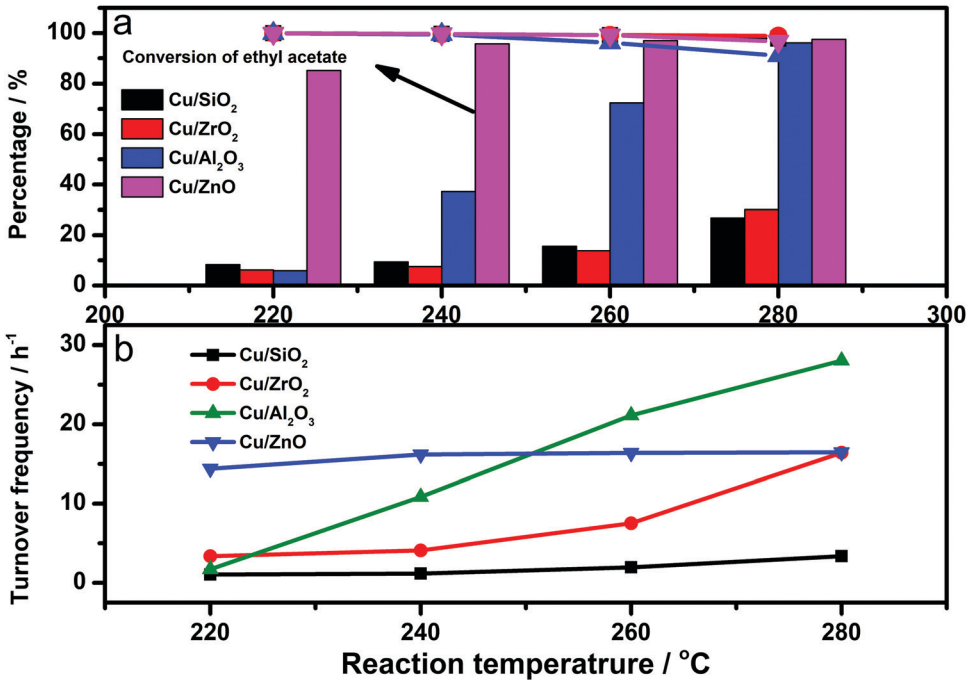

Fig. 6 The catalytic performance (a) and turnover frequencies (b) of the catalysts at reaction conditions (T = 220, 240, 260 and 280 °C): P = 2.5 MPa, n(H_2)/n(ethyl acetate) = 40 (molar ration), m(H_2O)/m(ethyl acetate)/m(ethanol) = 5/91/4 (mass ration) and LHSV of ethyl acetate = 1 h^{-1}.

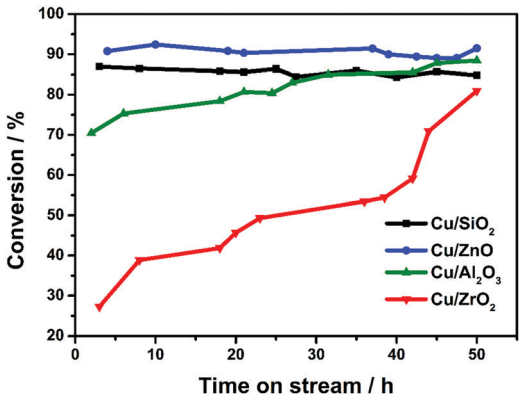

Fig. 7 The catalytic performances of all catalysts at reaction conditions: T = 240 °C (Cu/ZnO) or 280 °C (Cu/SiO_2, Cu/Al_2O_3, Cu/ZrO_2), P = 2.5 MPa, n(H_2)/n(ethyl acetate) = 40 (molar ration), pure ethyl acetate and LHSV of ethyl acetate = 1 h^{-1}.

difficult to be reduced at the same reduction conditions, and further resulting in a small number of active sites. Our previous studies have confirmed that the competitive adsorption between water and ethyl acetate existed in the ethyl acetate hydrogenation reaction.[18] The high number of active sites played an important role in the activity of ethyl acetate hydrogenation at reaction condition containing water.[17] Therefore, the conversion of Cu/Al_2O_3 and Cu/ZrO_2 catalysts were relatively low due to the incomplete reduction of CuO, and the conversion increased with the reaction time because of the further reduction of copper oxides under the reaction conditions.

As mentioned above, an obvious effect on the activity of the Cu/SiO_2 catalyst could be found from Fig. 6 and Fig. 7. From Fig. 6, it was found that the Cu/SiO_2 catalyst had just 30% conversion of ethyl acetate at reaction condition (280 °C) containing water. However, 87% conversion was obtained for the Cu/SiO_2 catalyst at reaction condition no-containing water, and no induction period was observed from Fig. 7. This phenomenon showed that water had a great effect on the hydrogenation performance of the Cu/SiO_2 catalyst. A published study has demonstrated that the doping of Fe, Co, Ni and Zn into the Cu/SiO_2 catalyst could form crystal defects at the border of copper species, and the doped metal species were seen as active sites of hydrogenation.[17] Furthermore, the adsorption/reaction sites with complementary chemical properties could be obtained in a metal–oxide interface.[37] Moreover, Ding *et al.* found that the formation of Cu–M_xO_y (M = Zn, Zr, Al) interfaces was beneficial to ethyl ester hydrogenations.[32] Therefore, more active sites were obtained for the Cu/ZnO, Cu/Al_2O_3 and Cu/ZrO_2 catalysts than that of the Cu/SiO_2 catalyst due to the formation of Cu–M_xO_y (M = Zn, Zr, Al) interfaces. Also, competitive adsorption existed between water and ethyl acetate on the active sites.[18] Therefore, the great negative impact on the Cu/SiO_2 catalyst was observed due to the existence of water. However, the strong interactions and big particle sizes for the Cu/Al_2O_3 and Cu/ZrO_2 catalysts were bad for the catalytic performance, so that they showed worse hydrogenation performances than that of the Cu/ZnO catalyst. That is, proper interaction, relatively small particle size and the formation of Cu–Zn_xO_y interfaces were responsible for the Cu/ZnO catalyst to exhibit good water-tolerant hydrogenation performance.

4. Conclusion

In this study, we chose SiO_2, ZnO, ZrO_2 and Al_2O_3 as supports to study the effects of supports on the hydrogenation and water-tolerance of copper catalysts. The results demonstrated that the strong interactions and channel structures had great effects on the catalytic activity of copper catalysts. The strong interactions between copper and supports hindered the reduction of copper oxides resulting in a low catalytic activity. Furthermore, the formation of Cu–M_xO_y (M = Zn, Zr, Al) interfaces were also seen as the active sites of hydrogenation, so that their water-tolerant hydrogenation performance was better than that of the Cu/SiO_2 catalyst. The Cu/ZnO catalyst, which possessed an appropriate interaction between Cu and ZnO, showed a good hydrogenation and water resistance performance. This work provides a factual basis for the effects of supports on the hydrogenation and water resistance performance of copper catalysts, which would have a positive effect on industrial production.

Conflicts of interest

The authors declare no competing financial interest.

Acknowledgements

This work was supported by the Natural Science Foundation of Shandong Province (ZR2020MB030 and ZR2020QB049), the Science and Technology Research Program for Colleges and Universities in Shandong Province (J18KA107) and the Key Research and Development Program of Shandong Province (2018GGX107010).

References

1 J. L. Gong, H. R. Yue, Y. J. Zhao, S. Zhao, L. Zhao, J. Lv, S. P. Wang and X. B. Ma, Synthesis of ethanol via syngas on Cu/SiO_2 catalysts with balanced Cu^0–Cu^+ sites, *J. Am. Chem. Soc.*, 2012, **134**(34), 13922–13925.

2 X. A. Li, X. G. San, Y. Zhang, T. Ichii, M. Meng, Y. S. Tan and N. Tsubaki, Direct synthesis of ethanol from dimethyl ether and syngas over combined H-mordenite and Cu/ZnO catalysts, *ChemSusChem*, 2010, **3**(10), 1192–1199.

3 Y. F. Zhu, X. Kong, X. Q. Li, G. Q. Ding, Y. L. Zhu and Y. W. Li, Cu nanoparticles inlaid mesoporous Al_2O_3 as a high-performance bifunctional catalyst for ethanol synthesis via dimethyl oxalate hydrogenation, *ACS Catal.*, 2014, **4**(10), 3612–3620.

4 Z. Chen, J. Zhang, M. Abbas, Y. Xue, J. Sun, K. Liu and J. Chen, Effect of configuration addition of precursors on structure and catalysis of Cu/SiO_2 catalysts prepared by ammonia evaporation–hydrothermal method, *Ind. Eng. Chem. Res.*, 2017, **56**(33), 9285–9292.

5 Y. Wang, Y. L. Shen, Y. J. Zhao, J. Lv, S. P. Wang and X. B. Ma, Insight into the balancing effect of active Cu species for hydrogenation of carbon–oxygen bonds, *ACS Catal.*, 2015, **5**(10), 6200–6208.

6 K.-i. Muto, N. Katada and M. Niwa, Complete oxidation of methane on supported palladium catalyst: Support effect, *Appl. Catal., A*, 1996, **134**(2), 203–215.

7 I. A. Fisher and A. T. Bell, In situ infrared study of methanol synthesis from H_2/CO_2 over Cu/SiO_2 and $Cu/ZrO_2/SiO_2$, *J. Catal.*, 1997, **172**(1), 222–237.

8 S. Storsaeter, O. Borg, E. A. Blekkan, B. Totdal and A. Holmen, Fischer-Tropsch synthesis over re-promoted co supported on Al_2O_3, SiO_2 and TiO_2: Effect of water, *Catal. Today*, 2005, **100**(3-4), 343–347.

9 J. A. Rodriguez, P. Liu, J. Hrbek, J. Evans and M. Perez, Water gas shift reaction on Cu and Au nanoparticles supported on $CeO_2(111)$ and $ZnO(000\bar{1})$: Intrinsic activity and importance of support interactions, *Angew. Chem., Int. Ed.*, 2007, **46**(8), 1329–1332.

10 W. W. Lonergan, T. Wang, D. G. Vlachos and J. G. Chen, Effect of oxide support surface area on hydrogenation activity: Pt/Ni bimetallic catalysts supported on low and high surface area Al_2O_3 and ZrO_2, *Appl. Catal., A*, 2011, **408**(1), 87–95.

11 Y. He, J. Fan, J. Feng, C. Luo, P. Yang and D. Li, Pd nanoparticles on hydrotalcite as an efficient catalyst for partial hydrogenation of acetylene: Effect of support acidic and basic properties, *J. Catal.*, 2015, **331**, 118–127.

12 M. M. Najafpour, M. Abasi, M. Hołyńska and B. Pashaei, Manganese oxides as water-oxidizing catalysts for artificial photosynthetic systems: The effect of support, *Int. J. Hydrogen Energy*, 2016, **41**(12), 5475–5483.

13 A. Vourros, I. Garagounis, V. Kyriakou, S. A. C. Carabineiro, F. J. Maldonado-Hódar, G. E. Marnellos and M. Konsolakis, Carbon dioxide hydrogenation over supported Au nanoparticles: Effect of the support, *J. CO_2 Util.*, 2017, **19**, 247–256.

14 H. M. Kim, B. J. Kim, W. J. Jang, J. O. Shim, K. W. Jeon, H. S. Na, Y. L. Lee, B. H. Jeon and H. S. Roh, Effect of support materials and Ni loading on catalytic performance for carbon dioxide reforming of coke oven gas, *Int. J. Hydrogen Energy*, 2019, **44**(16), 8233–8242.

15 K. Zhong and X. Wang, The influence of different precipitants on the copper-based catalysts for hydrogenation of ethyl acetate to ethanol, *Int. J. Hydrogen Energy*, 2014, **39**(21), 10951–10958.

16 Y. m. Zhu and L. Shi, Zn promoted Cu–Al catalyst for hydrogenation of ethyl acetate to alcohol, *J. Ind. Eng. Chem.*, 2014, **20**(4), 2341–2347.

17 Z. Chen, G. Zhu, Y. Wu, J. Sun, M. Abbas, P. Wang and J. Chen, The promotion effect of transition metals on water-tolerant performance of Cu/SiO_2 catalysts in hydrogenation reaction, *ChemistrySelect*, 2019, **4**(48), 14063–14068.

18 Z. Chen, H. Ge, P. Wang, J. Sun, M. Abbas and J. Chen, Insight into the deactivation mechanism of water on active Cu species for ester hydrogenation: Experimental and theoretical study, *Mol. Catal.*, 2020, **488**, 110919.

19 M. B. Gawande, A. Goswami, F. X. Felpin, T. Asefa, X. X. Huang, R. Silva, X. X. Zou, R. Zboril and R. S. Varma, Cu and Cu-based nanoparticles: Synthesis and applications in review catalysis, *Chem. Rev.*, 2016, **116**(6), 3722–3811.

20 Y. F. Zhu, Y. L. Zhu, G. Q. Ding, S. H. Zhu, H. Y. Zheng and Y. W. Li, Highly selective synthesis of ethylene glycol and ethanol via hydrogenation of dimethyl oxalate on Cu catalysts: I nfluence of support, *Appl. Catal., A*, 2013, **468**, 296–304.

21 K. K. Bando, K. Sayama, H. Kusama, K. Okabe and H. Arakawa, In situ FT-IR study on CO_2 hydrogenation over Cu catalysts supported on SiO_2, Al_2O_3, and TiO_2, *Appl. Catal., A*, 1997, **165**(1), 391–409.

22 J. Wambach, A. Baiker and A. Wokaun, CO_2 hydrogenation over metal/zirconia catalysts, *Phys. Chem. Chem. Phys.*, 1999, **1**(22), 5071–5080.

23 W. Di, J. H. Cheng, S. X. Tian, J. Li, J. Y. Chen and Q. Sun, Synthesis and characterization of supported copper phyllosilicate catalysts for acetic ester hydrogenation to ethanol, *Appl. Catal., A*, 2016, **510**, 244–259.

24 L. F. Chen, P. J. Guo, M. H. Qiao, S. R. Yan, H. X. Li, W. Shen, H. L. Xu and K. N. Fan, Cu/SiO_2 catalysts prepared by the ammonia-evaporation method: Texture, structure, and catalytic performance in hydrogenation of dimethyl oxalate to ethylene glycol, *J. Catal.*, 2008, **257**(1), 172–180.

25 K. Sing, D. H. Everett, R. A. W. Haul, L. Moscou, R. A. Pierotti, J. Rouquerol and T. Siemieniewska, Reporting physisorption data for gas/solid systems, *Pure Appl. Chem.*, 1985, **57**, 603–619.

26 M. Donohue and G. L. Aranovich, Classification of Gibbs adsorption isotherms, *Adv. Colloid Interface Sci.*, 1998, **76**, 137–152.

27 C. J. G. Van Der Grift, A. F. H. Wielers, B. P. J. Jogh, J. Van Beunum, M. De Boer, M. Versluijs-Helder and J. W. Geus, Effect of the reduction treatment on the structure and reactivity of silica-supported copper particles, *J. Catal.*, 1991, **131**(1), 178–189.

28 Z. Yuan, L. Wang, J. Wang, S. Xia, P. Chen, Z. Hou and X. Zheng, Hydrogenolysis of glycerol over homogenously dispersed copper on solid base catalysts, *Appl. Catal., B*, 2011, **101**(3), 431–440.

29 P. I. Kyesmen, N. Nombona and M. Diale, Heterojunction of nanostructured α-Fe_2O_3/CuO for enhancement of photoelectrochemical water splitting, *J. Alloys Compd.*, 2021, **863**, 158724.

30 S. H. Zhu, X. Q. Gao, Y. L. Zhu, Y. F. Zhu, H. Y. Zheng and Y. W. Li, Promoting effect of boron oxide on Cu/SiO_2 catalyst for glycerol hydrogenolysis to 1,2-propanediol, *J. Catal.*, 2013, **303**, 70–79.

31 J. F. Xu, W. Ji, Z. X. Shen, W. S. Li and X. Q. Xin, Raman spectra of CuO nanocrystals, *J. Raman Spectrosc.*, 1999, **30**(5), 413–415.

32 J. Ding and J. G. Chen, Synthesis of Cu–Zn–Zr–Al–O catalysts via a citrate complex route modified by different solvents and their dehydrogenation/hydrogenation performance, *RSC Adv.*, 2015, **5**(101), 82822–82833.

33 Z. W. Huang, F. Cui, H. X. Kang, J. Chen, X. Z. Zhang and C. G. Xia, Highly dispersed silica-supported copper nanoparticles prepared by precipitation-gel method: A simple but efficient and stable catalyst for glycerol hydrogenolysis, *Chem. Mater.*, 2008, **20**(15), 5090–5099.

34 Y. T. Liu, J. Ding, J. Q. Sun, J. Zhang, J. C. Bi, K. F. Liu, F. H. Kong, H. C. Xiao, Y. P. Sun and J. G. Chen, Molybdenum carbide as an efficient catalyst for low-temperature hydrogenation of dimethyl oxalate, *Chem. Commun.*, 2016, **52**(28), 5030–5032.

35 Z. Huang, F. Cui, H. Kang, J. Chen, X. Zhang and C. Xia, Highly Dispersed silica-supported copper nanoparticles prepared by precipitation−gel method: A simple but efficient and stable catalyst for glycerol hydrogenolysis, *Chem. Mat.*, 2008, **20**(15), 5090–5099.

36 I. Platzman, R. Brener, H. Haick and R. Tannenbaum, Oxidation of polycrystalline copper thin films at ambient conditions, *J. Phys. Chem. C*, 2008, **112**(4), 1101.

37 J. Graciani, K. Mudiyanselage, F. Xu, A. E. Baber, J. Evans, S. D. Senanayake, D. J. Stacchiola, P. Liu, J. Hrbek, J. F. Sanz and J. A. Rodriguez, Highly active copper-ceria and copper-ceria-titania catalysts for methanol synthesis from CO_2, *Science*, 2014, **345**(6196), 546–550.

